Elsevier Editorial System(tm) for Applied Energy

Manuscript Draft

Manuscript Number:

Title: Experimental and numerical study of a paraffin with a wide-range phase change for thermal energy storage

Article Type: Research Paper

Keywords: Latent heat storage; Natural Convection; OpenFOAM; Thermal modeling

Corresponding Author: Mr. Cecil Antonio Vega, Jr. Chemical Engineer

Corresponding Author's Institution: Universidad de Concepción

First Author: Cecil Antonio Vega, Jr. Chemical Engineer

Order of Authors: Cecil Antonio Vega, Jr. Chemical Engineer; Óscar C Pinto, Jr. Chemical Engineer; Alfredo L Gordon, PhD in Chemical Engineering

Abstract: Paraffins are useful as phase change materials (PCMs) in thermal energy storage (TES) systems for a variety of applications such as solar energy capture or waste heat recovery. However, there remain knowledge gaps concerning the evaluation of paraffins with non isothermal phase change for latent TES systems. Therefore, an experimental and numerical analysis of the effects of natural convection and phase transition temperature range is presented for a wide-range phase change paraffin. The paraffin was characterized by temperature-history method and tested in a finned shell-and-tube heat exchanger. The experimental test section is modelled with CFD simulations on the open source framework OpenFOAM and the melting and solidification fronts between fins are analysed. Experimental results exhibit differences between the melting period in the temperature profiles recorded in the storage unit and in characterization. The combined study highlights that local natural convection is key to explain the shape of the temperature profiles since it deforms the melting front and promotes a higher temperature gradients between liquid and solid phases.

***Highlights (for review)**

Highlights

A wide-range phase change paraffin was characterized by T-history method.
The paraffin was tested in a finned latent thermal energy storage (LTES) system.
The melting and solidification fronts between fins were numerically studied.
Differences between T-history and LTES melting temperature profiles were observed.
Natural convection promotes melting interface evolution and temperature gradients.

*Manuscript
Click here to view linked References

Experimental and numerical study of a paraffin with a wide-range phase change for thermal energy storage

Cecil Vega[a,*], Oscar Pinto[a], Alfredo Gordon[b]

[a] *Unidad de Desarrollo Tecnologico, Universidad de Concecpion, Coronel, Chile*
[b] *Facultad de Ingenieria Quimica, Universidad de Concepción, Concepcion, Chile*

Abstract

Paraffins are useful as phase change materials (PCMs) in thermal energy storage (TES) systems for a variety of applications such as solar energy capture or waste heat recovery. However, there remain knowledge gaps concerning the evaluation of paraffins with non isothermal phase change for latent TES systems. Therefore, an experimental and numerical analysis of the effects of natural convection and phase transition temperature range is presented for a wide-range phase change paraffin. The paraffin was characterized by temperature-history method and tested in a finned shell-and-tube heat exchanger. The experimental test section is modelled with CFD simulations on the open source framework OpenFOAM and the melting and solidification fronts between fins are analysed. Experimental results exhibit differences between the melting period in the temperature profiles recorded in the storage unit and in characterization. The combined study highlights that local natural convection is key to explain the shape of the temperature profiles since it deforms the melting front and promotes a higher temperature gradients between liquid and solid phases.

Keywords: Latent heat storage, Natural Convection, OpenFOAM, Thermal modeling,

*Corresponding author
Email address: cevega@udec.cl (Cecil Vega)

Nomenclature

Abbreviation

CFD	computational fluid dynamics
HTF	heat transfer fluid
LTES	latent thermal energy storage
PCM	phase change material
TES	thermal energy storage

List of Symbols

C_p	specific heat capacity (J kg^{-1} K^{-1})
C_u	large constant in Darcy type source term (kg m^{-3} s^{-1})
g	gravitational acceleration (m s^{-2})
H	total enthalpy (J kg^{-1})
k	thermal conductivity (W m^{-1} K^{-1})
P	pressure (Pa)
Pe	peclet number
q	small numerical constant in porosity function
S_p	darcy type source term in momentum equations (kg m^{-2} s^{-2}))
S_u	buoyancy source term in momentum equations (kg m^{-2} s^{-2}))
T	temperature (K)
t	time (s)
u	velocity (m s^{-1})

Greek Symbols

α	melt fraction
β	volumetric expansion coefficient (K^{-1})
Λ	Latent heat of fusion (J kg^{-1})
ρ	density (m^3 s^{-1})

Subscripts

l	liquid/liquidus
m	mean temperature
s	solid/solidus

1. Introduction

The use of latent thermal energy storage (LTES) reduces the mismatch between supply and demand and also improves the performance and reliability of energy systems [1]. Specifically, the advantages of heat storage using phase change materials (PCMs) have been demonstrated many times in the past because of its high storage densities and narrower operating temperatures, allowing a higher heat transfer rate compared to sensible heat transfer. Many existing applications incorporate PCMs, such as thermal management in building [2, 3, 4], industrial waste heat recovery and domestic hot water applications [5, 6, 7]. Paraffins, which are saturated hydrocarbons with C_nH_{2n+2} formula, are broadly used for the aforementioned applications. Several studies have already reported and demonstrated desirable properties which make this organic PCM suitable for LTES such as high latent heat storage capacities and negligible subcooling [1]. Furthermore, they are considered as non-toxic, ecologically harmless, non-reactive and are compatible with metal containers as they do not promote corrosion and repeated cycling across the solid–liquid transition does not induce phase separation [8]. However, there are also some undesirable properties that limit the potential capabilities of this material. Such major drawbacks are the large volume changes during phase transition and that a large surface area is needed as they have low thermal conductivity [9]. The optimal design of a LTES is a problem that involves the design of the system in regards to the PCM properties, and several designs were investigated by many authors [10, 11, 12, 13, 14, 15, 16, 17, 18, 19, 20, 21]. Amongst them, the shell-and-tube heat exchanger accounts for more than 70% of previously published papers dealing with LTES [5]. For a typical configuration, as studied experimentally by Akgün et al. [10], a heat transfer fluid (HTF) is pumped through the inner tubes and the outside void space is filled with PCMs for energy storage. However, the low thermal conductivity of the available PCM requires the development of efficient heat exchangers.

In order to address this issue, several modifications to the classic design have been proposed in order to improve the global heat transfer coefficient between PCM and HTF [13, 16, 19]. In general, both computational fluid dynamic (CFD) and experimental studies of LTES are nowadays the most useful tools to improve configuration of LTES and evaluate their phase change behavior and performance of PCMs. Development of a numerical tool for the optimization of geometric configuration and performance evaluation of LTES prototype is an ideal solution to reduce experimental efforts. However the mathematical modeling often proves to be problematic. The major problems involved in the modeling are (i) inclusion of latent heat of PCM, (ii) natural convection of the melt and (iii) conjugate heat transfer between the PCM and HTF. Because of these complications, researchers try to focus on one aspect of the heat transfer phenomena, such as flow direction, geometry or natural convection in the paraffin, whilst trying to keep all other variables constant.

Logeon et al. [22] studied a shell-and-tube heat exchanger both experimentally and numerically. The impact of natural convection of HTF flow direction was studied, and it was concluded that a top injection for charge and a bottom one for discharge are recommended. To achieve this, flow conditions were set to laminar, which is a common practice among many authors. Similarly, Soupart [23] compared different configuration, among them vertical fins, annular fins, one horizontal tube and a multi tube. A novel technique for comparing different geometries according to different parameters was proposed. The addition of fins proved to be an elegant solution for heat transfer enhancement due to it low cost of construction and easy to fabricate. This configuration was numerically evaluated by Jmal et al. [14], and highlights the important role of natural convection in the thermal performance. Subsequently, Yang et al. [17] studied numerically the role of annular fins and their effect over thermal performance of PCM through numerical simulations including natural convection. The remarkable of this study is the optimization of both interval and thickness of fins.

On the other hand, other authors try to focus on flow conditions, such as the experimental study conducted by Martinelli et al. [5] on a finned tube. As mentioned, a low-Reynolds-number flow combined with a high Rayleigh number can result in mixed convection which can increase (aided mixed convection) or decrease (opposed mixed convection) the heat transfer coefficient. In a study done by Colella et al. [24], in spite the Reynolds number was found to be between 500 to 2000, their operating conditions show a high Rayleigh number. the flow regime is not laminar as expected and considered in the study, but characteristic of a "turbulent flow of mixed convection". Wang et al. [15] also studied various flow conditions on a finned tube. It was stated that the energy efficiency ratio and the heat storage rate are larger for laminar state than that in a turbulent state. However, natural convection was neglected.

For instance, all of the aforementioned authors use almost pure paraffins, such as RT35HC. This paraffin is widely used since it provides a narrow range of phase change temperature between 34 and 36 $°C$, and thus the melting or solidification process can be visualized easily in the PCM temperature profiles. Nevertheless, as stated by Gasia et al. [7], due to the high cost of manufacturing, only technical grade paraffins (mixtures of many hydrocarbons) are used for LTES purposes. In that study, the technical grade paraffin RT58, with a melting range between 51 to 59 $°C$ is used. However, the shape the temperature are profiles observed in their pilot plant are different than the ones obtained by the laboratory analyses. Furthermore, the shape of the temperature profiles of technical grade paraffins in a heat exchanger are different from the ones obtained by using pure paraffins, such as the temperature jumps observed by Merlin et al. [6] whilst studying the paraffin RT60.

Nevertheless, the literature survey demonstrates that few studies have taken an in depth look at the temperature profiles observed by technical grade paraffins. The present study therefore aims

to deal with this observations. An experimental loop was built that enables storage and recovery of energy in an annular PCM heat exchanger placed vertically. A technical grade paraffin was chosen as the storage medium, laboratory and experimental results are compared. Furthermore, simulations of convection dominated phase change are performed to help explaining the phenomena. Turbulent HTF flows conditions in the LTES unit are taken into account numerically through a low Reynolds turbulence.

2. Matherial and methods

2.1. Characterization of PCM

A commercial paraffin named RT47 was used as PCM material in this work. The PCM was provided by Rubitherm Technologies GmbH (Germany). Table 1 shows the main properties of the PCM according to the information provided by the supplier.

Table 1: Thermo-physical properties of commercial paraffin RT47 according to the manufacturer

Properties	Values
Phase change temperature range ($°C$)	41-48
Latent heat (J kg^{-1})	165000
Density (liquid) (kg m^{-3})	760
Specific heat capacity (solid/liquid) (J $^{-1}$ kg K^{-1})	2000
Thermal conductivity (solid/liquid) (W m^{-1} K^{-1})	0.2
Dynamic viscocity (kg m^{-1} s^{-1})	0.003465
Thermal expansion coefficient (K^{-1})	0.000848

Logeon et al. [22] and several authors mention that the PCM physical data given by suppliers

are of uncertain accuracy. Therefore, measurement of the phase change temperature range, the thermal conductivity (k), the specific heat capacity (C_p) and latent heat are necessary to precisely model heat exchange in the PCM. Accordingly, measurements were carried for both liquid and solid states.

The thermal conductivity is measured through the transient line source method using a KD2-Pro instrument with a needle model KS-1. The thermal behavior, that is, phase change temperature, heat capacity, and latent heat of fusion, is measured by *T-history* method proposed by Yinping et al. [25] with the modifications of Lázaro et al. [26] and Rathgeber et al. [27]. An insulated box (0.85 m x 0.39 m) provided with an external air circulation system was used as test rig. Both temperature and flow rate of the air were controlled through an external fan and a heater source. Thus, a controlled forced convection is introduced into the system. Two glass test tubes with an outer diameter of 13 mm, thickness of 2.5mm and height of 250 mm were used as sample port. Distilled water was used as reference material. Both reference material and PCM were kept at an initial temperature and then simultaneously introduced in the test rig exposed at the setup temperature. The temperature of materials was measured using RTD (PT100) sensors located at the center of the test tube and frequency of data acquisition was 0.1 Hz. The enthalpy change of RT47 was calculated using the methodology proposed by Marín et al. [28], this means to do a balance energy between the reference material and the PCM sample using a time interval of $t(T_i)$ and $t(T_{i+1})$. In this case the interval temperature was 1°C. This implies the assumption of heat transfer coefficients for PCM and reference material are both equal over a same temperature interval. Even though this is not completely right, it provides a good approximation.

2.2. Experimental setup

The experimental setup is composed of a test rig where the heat exchanger is located, several instrumentation devices and a hydraulic loop with two water baths with adjustable pumps. One bath is used as a cooler and the second is used as a heater. Both, cold and hot flow run in parallel, whilst one flows through the test rig, the second is bypassed. Consequently, it is possible to alternate between charging and discharging processes. Furthermore, the experimental set up enables upward and downwards flows.

The PCM storage system is shown in Fig. 1 and is composed of a polycarbonate shell of 70 mm diameter and 3 mm thickness placed around a finned copper tube. The inner and outer diameter of the tube are 19.9 mm and 22.2 mm respectively. The fins are 65 mm in diameter, 0.5 mm in thickness, and were soldered with silver with 11 mm spacing along the tube starting from 38 mm from the bottom of the heat exchanger. The heat exchanger is placed vertically and has a total length of 510 mm. The HTF flows into the inner tube through a metal tube at the top or bottom of the heat exchanger, and 1300 g of PCM fills up the annular space.

In the experiments, the temperature evolutions of the PCM at six locations are monitored by using temperature sensors PT-100 with a diameter of about 1 mm. These are distributed at two radials positions, denoted by "1" and "2" respectively, at 21 and 32.5 mm from the centre of the heat exchanger, on three different heights, denoted as sections "A", "B" and "C", respectively at 0.138 m, 0.25 m and 0.438 m from the bottom of the heat exchanger, as shown in Fig. 1. The temperature sensors PT-100 were locked by using tube fittings on threads made in the surface of the shell. However, the radial and axial positions obtained during threading were not exactly the expected ones. The HTF temperatures at inlet and outlet of the tubes in the LTES unit are also monitored temperature sensors PT-100. The temperatures of the monitoring points are recorded

every 1 s by a data acquisition system.

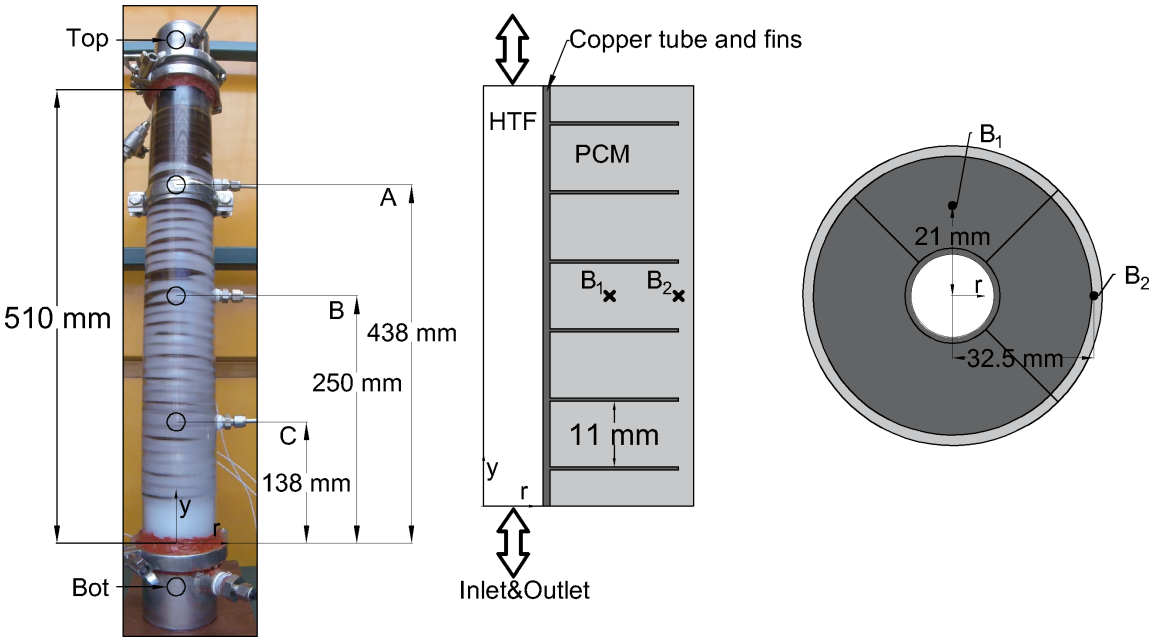

Figure 1: Thermocouple positions in the test section

2.3. Experimental procedure

Experimental scheme is the same as used by several other authors [22, 6, 29], and is described as follows: Before starting the charging process, a warming process was required to make the PCM be uniform and homogeneous at an initial temperature of 64 °C charging. Water from the cold bath flows through the LTES unit for several minutes until the LTES unit reaches the initial temperature condition of 23 °C. Then the heat charging process starts, the HTF from the hot water bath is injected from the top of the LTES unit and the temperature of the paraffin increases. The charging process was considered to be finished when all the monitored temperatures are at an steady state above the melting point. Then, a reverse process took place to carry out the discharging process, where the PCM initial temperature is 64 °C and HTF is injected from the bottom of the LTES

with an inlet temperature of 24 °C.

The average temperature in the PCM and the thermal power of the HTF are introduced to identify the different steps occurring in the charging and discharging processes. The average temperature of the PCM is estimated as the mean temperature in each division (A,B or C). These temperatures are obtained as a weighted mean of the temperatures measured by the sensors relative to the area covered, which is 0.8 for the sensors at radial position 1 and 0.2 or sensors at radial location 2. The thermal power Φ is calculated by using the temperature difference between the inlet and outlet ΔT and the mass flow rate $\dot{m}$.

$$\Phi = \dot{m} \cdot C_{p_{HTF}} \Delta(T_{in} - T_{out}) \tag{1}$$

In regards to the water inlet velocity, it was carefully selected given the experimental setup so as to avoid unstable flow conditions. The HTF injection velocity must be small enough as recommended by Longeon et al. [22] in their experiments with a similar sized shell and tube heat exchanger in order to achieve a temperature gradient between inlet and outlet of water. However, by taking into account the experiments done by Martinelli et al. [5] on flow conditions in a similar sized finned tube heat exchanger, laminar-turbulent transitional conditions must be avoided since this flow regime can easily become unstable, is highly unpredictable and sometimes unreproducible. Thus, the average injection velocity of water was chosen to be 0.019 m s^{-1} and is considered to be under turbulent conditions with mixed convective heat transfer mode. The resulting flow regime was obtained by looking at the Metais and Eckert's [30] diagram showing the different zones were natural, forced and mixed convection for turbulent and laminar flow through in vertical tubes. As a matter of fact, superior velocities would decrease the temperature gradient between inlet and outlet of water and inferior velocities would lead to laminar-turbulent transitional conditions.

3. Numerical model

3.1. Mathematical model

The experimental test section is modelled using a 2D axisymmetric geometry and is exactly the same as represented in Fig. 1. Therefore, the three zones modelled correspond to the PCM, the HTF tube and the copper tube wall and fins. Modelling and simulations are carried out in the open source framework OpenFOAM [31]. OpenFOAM is a C++ based programme library offering numerous tools to solve various computational fluid dynamics (CFD) tasks.

For the numerical simulations performed in this paper, the following assumptions are made:

- The computational domain consists of a half a the two-dimensional representation of the heat exchanger given its axial symmetry.
- The HTF and liquid paraffin are considered as incompressible Newtonian fluid. The latter is due to the fact that density variations in the liquid paraffin are small, variations in density have no effect on the flow field, except that they give rise to buoyancy forces.
- Thermo-physical properties are constant.
- The initial temperature in the heat exchanger is constant and uniform. The inlet flow velocity and inlet temperature of the HTF are set by the values obtained during the experimentation.

Numerical modeling of a LTES unit has been done by several other authors [17, 32, 23, 29, 22, 33]. For instance, Yang et al. [17] studied numerically a similar sized finned tube heat exchanger. The model developed is based on a coupled conjugate heat transfer problem, which simultaneously solves the flow behavior of HTF and phase change behavior of PCM. Similar assumptions and the same governing equations were given. In general, numerical modeling of a LTES consist in adapting an

existing sensible heat based model for a latent heat storage based model. The biggest challenge and also the main variations between numerical studies is the incorporation of latent heat required to melt/solidify the PCM. The equations used in the present work are shown below.

3.2. Governing equations

The enthalpy-porosity method as proposed by Voller and Prakash [34] is used to describe the phase change process of the PCM. The governing equations consisting of the continuity, momentum, and energy equations are presented below [35]:

Conservation of mass:

$$\nabla \cdot \vec{u} = 0 \tag{2}$$

Conservation of momentum:

$$\rho(\frac{\partial \vec{u}}{\partial t} + (\vec{u} \cdot \nabla)\vec{u}) + \nabla P = \mu \nabla^2 \vec{u} + \vec{S_u} + \vec{S_p} \tag{3}$$

Conservation of energy:

$$\rho(\frac{\partial H}{\partial t} + \nabla \cdot (\vec{u}H)) = \nabla \cdot (k \nabla T) \tag{4}$$

For the conservation of mass and momentum equations, u is the velocity, P is the pressure, t is the time and β is the expansion coefficient of liquid relevant to a reference temperature T_{ref}. In the energy equation, T is the temperature, k the thermal conductivity and H the total enthalpy. The source term $\vec{S_u}$ is added to the momentum equation and allows to take into account the changes in density (ρ) causing natural convection without the need to solve for the full compressible formulation of the Navier-Stokes equations. It is implemented through the Boussinesq approximation [36], which states that the density variation is only important in the buoyancy term, and can be neglected in

the rest of the equation, as shown by Eq. (5).

$$\vec{S_u} = \rho \vec{g} \beta (T - T_r ef) \tag{5}$$

To nullify the velocities in the solid region of the PCM, Darcy law's source term [34, 37] is added to the momentum equation, which is given by Eq. (6). This is a porosity model that allows to represent the phase change by considering the solid-liquid transition region as a porous or mushy zone with a liquid fraction α between 0 and 1.

$$\vec{S_p} = C_u \frac{(1-\alpha)^2}{(\alpha^3 + q)} \vec{u} \tag{6}$$

The mushy zone constant (C_u) defines the transition of velocity in the mushy region and (q) is a small constant to avoid division by zero when the melting fraction in the PCM (α) is zero. For higher values of the mushy zone constant, the damping curve becomes steeper, and the velocity drops to zero faster as the material solidifies. Very large values of mushy zone constant may cause the solution to fluctuate as elements interchangeably melt and solidify with minor perturbations in the liquid volume fraction.

The non-linear relation between the total enthalpy and temperature in the PCM is approximated by a piecewise linear function. As proposed by Voller and Prakash [34], the total enthalpy can be segregated as sensible and latent heat:

$$H = C_p T + H_\Lambda \tag{7}$$

Within the source based method discussed in the article written by Voller and Prakash [34], the latent heat changes between the solidus temperature (T_s) and liquidus temperature (T_l) and is

expressed as:

$$H_\Lambda = \left\{ \begin{array}{cc} \Lambda, & T > T_l \\ \Lambda \cdot \alpha_l, & T_l \geq T \geq T_s \\ 0, & T < T_s \end{array} \right\} \tag{8}$$

By combining (8) and the energy equation presented in (4), the rearranged energy equation reads [34]:

Conservation of energy:

$$\rho C_p(\frac{\partial T}{\partial t} + \nabla \cdot (\vec{u}T)) = k(\nabla \cdot (\nabla T) - \rho(\frac{H_\Lambda}{\partial t} + \nabla \cdot (\vec{u}H_\Lambda)) \tag{9}$$

In the source based method, the term $\rho(\frac{H_\Lambda}{\partial t} + \nabla \cdot (\vec{u}H_\Lambda))$ is the latent heat source term computed and corrected using an iterative approach [38]. The usage and numerical integration of this approach in OpenFOAM is discussed in detail by Kasibhatla et al. [39] to model numerically the melting and settling of PCM in a capsule is implemented. This model was adapted to implement non isothermal phase change by changing the liquid fraction update definition as shown below:

$$\alpha_i^{n+1} = \alpha_i^n + URF \cdot \frac{C_p}{\Lambda}(T_i^n - T_m \cdot \alpha_p^n)) \tag{10}$$

In Eq (10), i is the cell being calculated, n + 1 is the present time step, n is the previous time step. The term T_m is the phase change temperature, $\frac{C_p}{\Lambda}(T_p^n - max(T_s, T_s + (T_l - T_s) \cdot \alpha_p^n))$ represents the fraction of the amount of energy contained in the fluid cell above melting point and URF is an under relaxation factor for the iteration steps, determined to be 0.7. It should be noted here that the choice of the URF influences the stability and accuracy of the solution and its value lie between 0 and 1. To take into account no isothermal phase change, the melting temperature T_m in Eq. 10 was changed to $max(T_s, T_s + (T_l - T_s) \cdot \alpha_p^n)$.

3.3. Initial and boundary conditions

Considering a computational domain represented as in Fig. 1, the boundary conditions are as follow: Initially ($t = 0$), the HTF domain is given zero velocity (no flow condition), and all the domains (PCM, HTF, and copper) are given a constant lower/higher temperature of 23 °C and 64 °C during charging and discharging process, respectively. At any time ($t > 0$), the HTF is injected from the top for the charging process and bottom for the discharging process with a variable temperature equivalent to the experimentally measured data from the temperature sensor located at the inlet. A constant fluid velocity of 0.019 m s^{-1} is defined at the HTF inlet. The outlet is set at atmospheric pressure and to account zero velocity on the HTF tube walls, no-slip boundary condition was used. The left wall for the computational domain is symmetrical and the top and bottom except the inlet and outlet are kept as adiabatic. For the right wall, the heat loss is estimated by the natural convection between the polycarbonate wall and the ambient air. To account for this part, the natural convective heat transfer between the shell and the ambient temperature is estimated iteratively. The value is determined to be 23 W m^2 K^{-1} during the since it provides the same thermal stratification is observed experimentally and numerically.

3.4. Numerical procedure

The complete numerical model is implemented in OpenFOAM v6 [31] and an uniform hexahedral structured grids are used to discretisize the HTF, copper tube and PCM domains represented in Fig. 1. The meshes are smaller on the periphery of the fins because this is where natural convection is most likely to establish and a cell expansion ratio of 0.1 in the radial direction of the HTF domain is used to take into account the layer between the copper tube and water.

The momentum and energy equations are discretized by the finite volume method. The pressure-velocity coupling is done by a combination of semi-implicit method for pressure linked equations

(SIMPLE) [35] and pressure implicit with splitting of operator (PISO) [40] namely PIMPLE algorithm is used to solve the segregated pressure and velocity equations. The experimental flow conditions described in section 2.3, which were found to be under turbulent conditions with mixed convective heat transfer mode, are modelled by using a Launder-Sharma Low-Re k-ϵ model [41]. Variable time step is used, where the convergence condition is given by Courant-Friedrich-Levy condition with a courant number equal to 0.6. The numerical results of each time step are obtained when the convergence criteria of the solutions are satisfied, and the convergence criteria for the residuals of continuity equation, velocity components and energy equation are 10^{-6}, 10^{-6} and 10^{-8}, respectively.

The influence of the grid number and time step on the numerical result is checked, and three different meshes of approximatively 100, 220 and 410 thousands grids are tested. By comparing the numerical results with different meshes, it is found that the mesh with a total number of $2.2{\cdot}10^6$ elements is good enough to obtain high accuracy since the predicted values exhibits a deviation less than 1.8% from the mesh with $4.1{\cdot}10^6$ elements. Furthermore, different values for the mushy zone constant C_u were tested, and it determined to be 10^6 since it provides the best similarity between the numerical and experimental curves.

4. Results and discussion

4.1. PCM thermal behavior

Results from the laboratory analyses are shown in Fig. 2. The PCM does not exhibit subcooling, however, it has a remarkable hysteresis both in the melting and freezing. The melting process starts at 38 °C, substantiated by an increase in partial enthalpy until it reaches a peak value (31.7 kJ kg^{-1} K^{-1}) at 41 °C. From that point on the partial enthalpy values decreases

until the melting process is considered finished at 47 °C. The freezing process starts at 47 °C and reaches a peak partial enthalpy value (48.5 kJ kg^{-1} K^{-1}) immediately after at 46 °C. Afterwards, a constant decrease in partial enthalpy is observed until 40 °C. Whilst a decrease can be observed from 40 °C to 38 °C, the freezing process experimentally was determined to be finished at 40 °C. The average heat storage capacity, which combines both latent and sensible heat during the phase change is 185.8 kJ kg^{-1} with a relative error of 8.5% in regards to the supplier information[42]. The thermal conductivity in the solid state measured at 30 °C is 0.190 ± 0.008 W $m^{-1}K^{-1}$. In the liquid state, the measured value at 65 °C is 0.241 ± 0.010 W m^{-1} K^{-1}, which are considerably higher in comparison to the solid state. The former difference in properties between phases are not stated by the manufacturer, and can lead to issues in further projects using RT47.

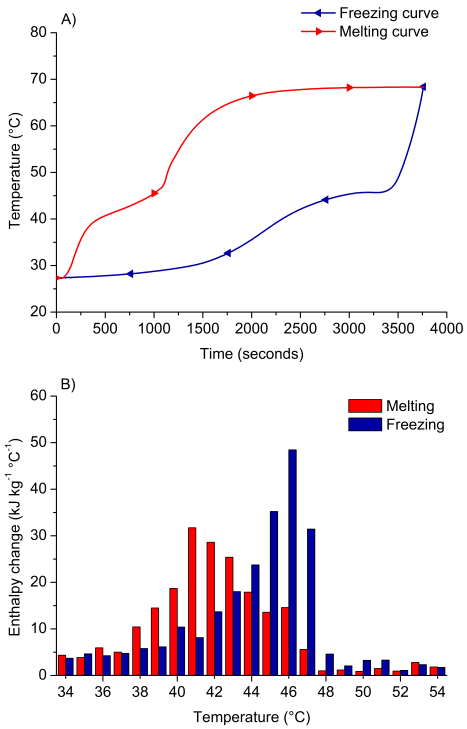

Figure 2: A) Temperature curves and B) entalphy change of RT-47 of T-history assays for melting process (red) and freezing process (blue).

In the present study, heat capacity and conductivity were decided to be kept constant and their mean values are respectively 2650 J kg^{-1}K^{-1} obtained by the *T-history* method and 0.216 W m^{-1} K^{-1} determined by conductivity measurements. Whilst the numerical results shown below can be improved by using variable heat capacity and conductivity, these values proved not be critical in the later results. However, the implementation of these variables can often lead to confusing results, were it's not quantifies the critical values that rule the phenomena. Besides, numerical models with variable heat capacity and conductivity are addressed in many others papers [29, 17].

4.2. Power profiles

The experimental and numerical results of the power released and absorbed by the HTF and the average temperature evolutions during the charging and discharging processes are shown in Fig. 3. At the beginning of both experiments, a maximum value in the power is observed. This is due to the fact that heat was mainly transferred to the metallic tubes bundle, which has a high thermal conductivity and the thermal gradient between the HTF and the PCM was at a maximum. Subsequently, as sensitive heating or cooling of the PCM takes place, the PCM average temperature increases whereas the power diminishes. This decline is higher during the discharging process because heat losses are involved. Besides, since the PCM is liquid, the natural convection is present. Immediately after, when the PCM started the phase change, the power decrease rate diminishes due to the increase of the PCM thermal resistance. The reason lies in the fact that the temperature difference between the HTF and PCM increases at a slower rate due to the involvement of latent heat as the melting or solidification process occurs. As the phase change completes, the power and the PCM average temperature reach a steady state. For the charging process, the power released remains at a constant value of (≈40 W) because heat losses are involved whereas in the discharging process there is no power absorbed by the HTF (≈0 W) because the average temperature of the PCM reaches HTF inlet temperature (23 °C).

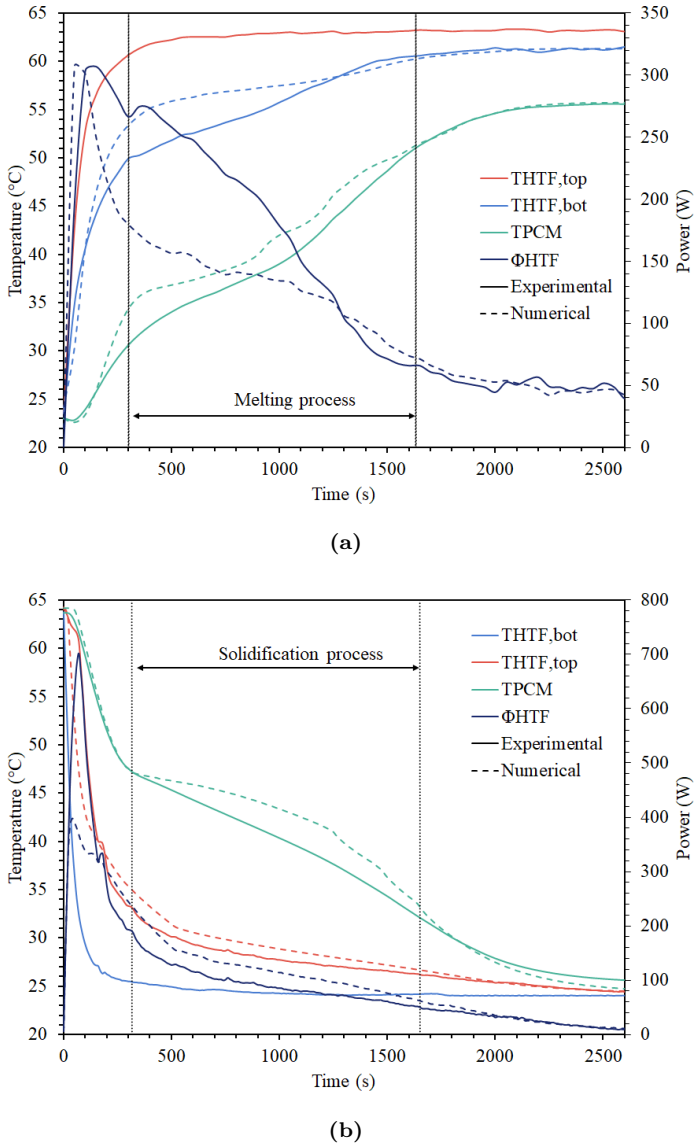

Figure 3: HTF power profiles and average PCM and HTF temperature profiles for (a) charging and (b) discharging processes.

By comparing numerical and experimental temperature for the power absorbed during the discharging process, it is apparent that the results are very similar. On the other hand, for the power

released during the charging process, the values reported numerically are lower in comparison to the experimental ones during the melting period. It should be noted that the numerical outlet of water is different from the experimental one, which is located at the metal tube at the top and bottom of the heat exchanger (Fig. 1). Thus, the heat losses occurring between the numerical outlet and the experimental outlet are not taken into account generating the discrepancies between the temperatures reported at the numerical and experimental HTF outlet and thus explaining the lower power value observed numerically. In regards to the PCM average temperature, although some discrepancies can be observed both for melting and solidification periods, the phase change is faithfully reproduced. Moreover, it appears that the experimental and numerical results are similar, which indicates that the overall process is numerically well represented.

4.3. Temperature evolutions

The individual temperature profiles used to calculate the PCM average temperature in Fig. 3 for the charging and discharging processes are shown in Fig. 4. Here, the temperature evolution of the PCM at locations A, B and C are shown for experimental and numerical results represented by a continuous and dashed line respectively.

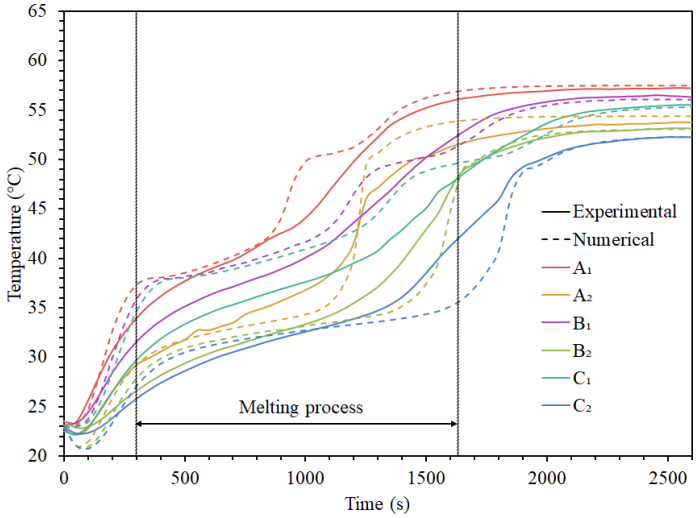

(a)

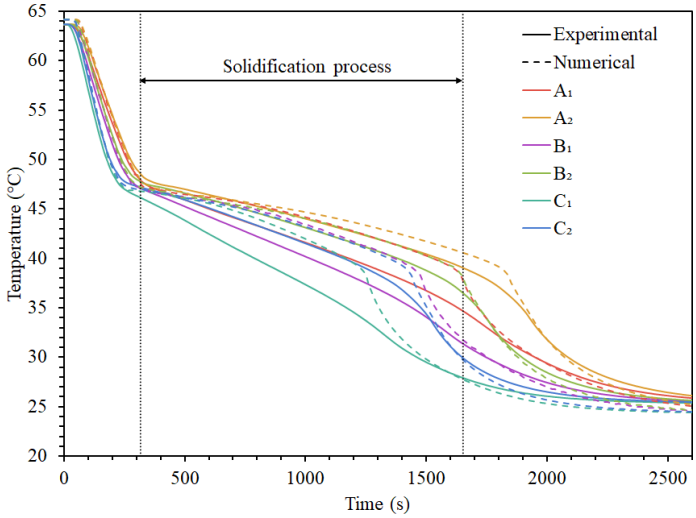

(b)

Figure 4: Experimental and numerical results of the PCM temperature profiles during the heat (a) charging and (b) discharging processes.

Sections "A", "B" and "C" are located at axial positions 0.138 m, 0.25 m and 0.438 m and subscripts "1" and "2" denote the two temperature sensors located in each section at radial positions 21 and 32.5 mm.

At the beginning of the charging process the numerical temperatures close to the shell (A_2,B_2,C_2) decrease slightly before it starts increasing. This is due to the fact that heat losses were modeled only by a heat transfer between the wall and the outside air. This value is higher in comparison to the experimental one because it takes into account the total heat transfer between the heat exchanger and the ambient. As the charging process occurs, the temperature at different radial or axial locations start to differ. If the section is closer to the top of the heat exchanger, the faster it heats up and has higher temperature gradients because they are closer from the HTF injection. Similarly, the temperature sensors located closer to the copper tube at the same radial location (A_1,B_1,C_1) increase faster than the ones closer to the shell (A_2,B_2,C_2). Following a similar pattern, the melting period seems to be offset and extended the farther the sensor is from the injection point. For instance, the melting process is not seen in B_2, where the temperature rises quickly from 36 °C at instant 1440 s. Analogously, a correlation between the visibility of the melting period and the proximity of the temperature sensor to the heat source (fins and tubes) has been reported by other authors whilst working with paraffins that melt in a narrow temperature range [32, 23, 22]. The reason given, is that the heat losses affect the sensors located in the periphery, where the melting occurs abruptly. Finally, the same thermal stratification is seen at all locations both experimentally and numerically.

For the discharging process, the experimental and numerical temperature profiles at different monitoring points during the first 400 s of the experiment are almost the same. Differences are seen only during the solidification period. Experimentally, it can be seen that the temperature decrease rate accelerates for lower temperatures, which in turn causes experimental results to be lower than their numerical counterparts. This can be correlated to the *T-history* results, where the partial enthalpy reduces as the temperature decreases. Numerically, the same trend is observed but less

markedly. However, variable latent heat was not implemented. In this case, this trend is due to the form of the solidification front, which will be explained in the next sections. Thus, the results observed experimentally might be a results of these two aforementioned factors. As opposed to the charging process, the discharging process is correlatable to the *T-history* results. However, it is important to distinguish that correlation does not imply causation. As seen numerically, whilst the same correlation is observed, the explanation given experimentally cannot be applied. By taking into account that for both numerically and experimentally, the shape of the temperature profiles in the same radial location is the same, an assessment of the aforementioned differences is done in the following section.

4.4. Effects of natural convection

The numerical visualization of the PCM average velocity fields between 2 fins at section B of the heat exchanger during the heat charging and discharging processes is shown in Fig. 5. For the heat charging process, numerical results indicate that natural convection is almost negligible during the initial stage because the PCM is mainly at solid phase. However, at instant 1180 s, a sufficient amount liquid is present in the inter fin space and a developed movement profile is observed. The thermal gradients generate a movement in the radial direction at a speed of about 0.4 mm s^{-1} along the melting front and along the tube and upper fin. Furthermore, heat losses delay the charging process, giving the opportunity for convective movements to be establish. As the melting process continues, this movement intensifies and the liquid accelerates along the heat sources until it reaches speeds of about 1 mm s^{-1} (Pe=113). At the end of the charging process, heat losses maintain this movement and provide a greater thermal stratification.

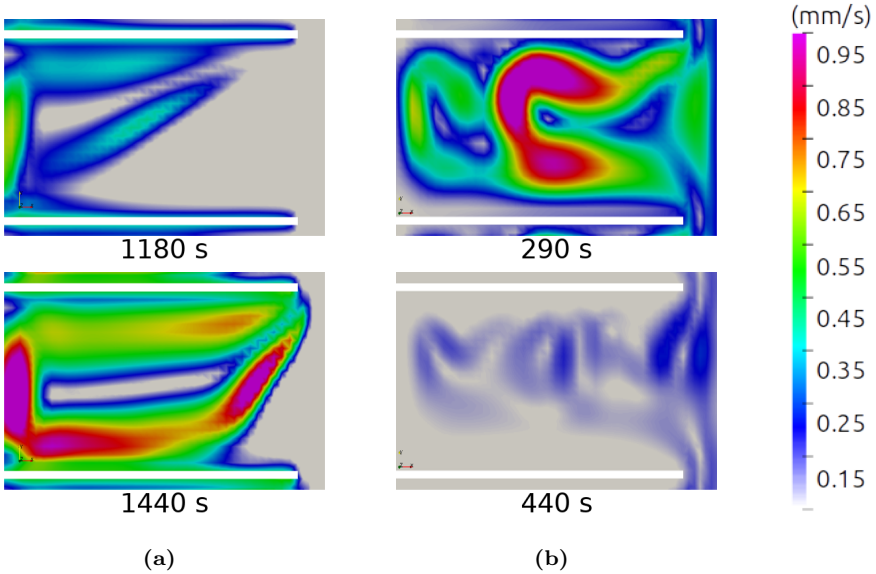

Figure 5: Average velocity field between the 2 fins at section B on the heat exchanger during the heat charging (a) and (b) discharging processes.

On the other hand, at the beginning of the discharging process, natural convection in the inter fin area takes place due to the temperature gradients generated by the heat losses and the cold water circulating through the system. Speed locally reaches values close to 1 mm s^{-1} as seen in instant 290 s which helps homogenizing the temperature around the inter fin area, as stated in the previous sections. From that point on, the movement dissipates fairly quickly as the solidification process occurs, where the fluid movements at 440 s are almost non existent and confined between regions that already solidified. Therefore, the discharging process can be simplified as a conductive process, the overall effect of natural convection is minor, mainly due to the fact that this heat transfer mechanism is short lived.

4.5. Melting front evolution

Fig. 6b shows the liquid fraction distribution between two fins at the section B, the squares represent the sensors location B_1 and B_2 which temperatures are shown in Fig. 6a.

After 480 s have elapsed since the beginning of the charging process, the temperature stabilizes, which is commonly correlated to the melting period. Numerically, the temperature at the beginning of this period in B_1 is 38 °C. Experimentally, the temperature is 36 °C, which is 2 °C lower to what is seen in the *T-history* results. Whereas the melting temperature has just been reached in B_1, the PCM that is contiguous to the heat source (tubes and fins) is already melted. Since the heat capacity and conductivity of the PCM are constant, the differences are due to the important thermal stratification provoked by heat losses inside the heat exchanger. If the PCM is closer to the heat source, the faster it will heat. Thus, the PCM that is contiguous to he heat source starts and finish the melting process faster than the PCM in location B_1. From instant 480 to 960 s, the temperature in B_1 and B_2 increases slightly whilst the melting front advances. Nevertheless, the stabilization period in B_1 ends before the temperature reaches the liquidus temperature (47 °C). In both experimental and numerical temperatures, an inflection point and then a quick temperature rise is seen at 960 s. However, the temperature is approximately 41 °C, which is 6 °C lower to what is reported in the *T-history* results. From that point on, the temperature start to rise quickly again, as seen at 1180 s. Thus, the end of the melting period and the beginning of sensitive heating of the liquid PCM is difficult to distinguish. This is most likely to occur when using paraffins which melts in a wide temperature range ($\approx$ 6 °C) such as the technical paraffin RT58 which was characterized and employed in a pilot plant by Gasia et al. [7]. However, the end of the melting period is distinguish clearly for more refined paraffins which melt in a narrower melt temperature range ($\approx$ 2 °C) such as RT35HC used by many studies [22, 32, 23]. Furthermore, it in spite that

the numerical model has a fixed melting range, numerical and experimental results are similar. In general, the temperature profiles for the melting process are hardly correlated to the *T-history* results. This is because in the *T-history*, the only heat transfer mechanism is conduction, whereas as seen by other authors, natural convection greatly affects the shape of the temperature profiles [14].

As shown in Fig. 5a, natural convection generates mixing in the melted PCM, allowing the heat transfer in the liquid PCM higher than the solid PCM where the only heat transfer mechanism is conduction, and acts as a resistance to the PCM further away in the radial direction of the melting front. Furthermore, since RT47 has a 10 °C difference between the liquidus and solidus temperatures. Thus, when the melting front arrives to B_1, the PCM at solid state or melting is exposed to the liquid PCM at a higher temperature, generating a quick temperature rise. This generates that the solidification plateau may be entirely skipped, as seen in B_2. The temperature remains stable until the front reaches it location at the instant 1440s, when the temperature in B_2 rises quickly from the solid PCM there to the temperature of the liquid PCM in the melting front.

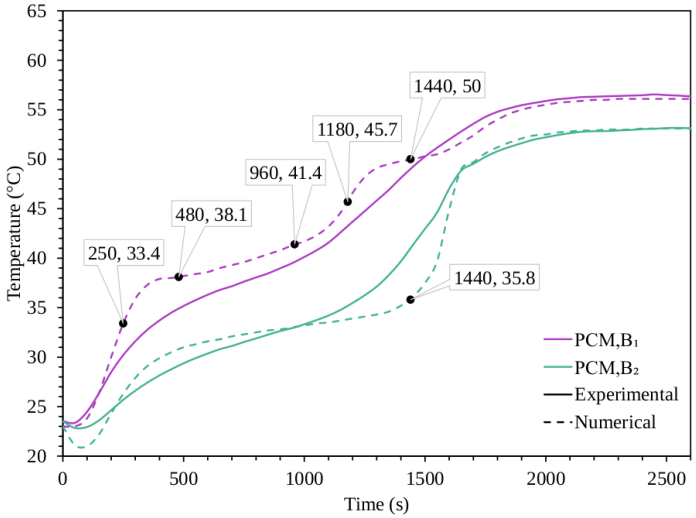

(a)

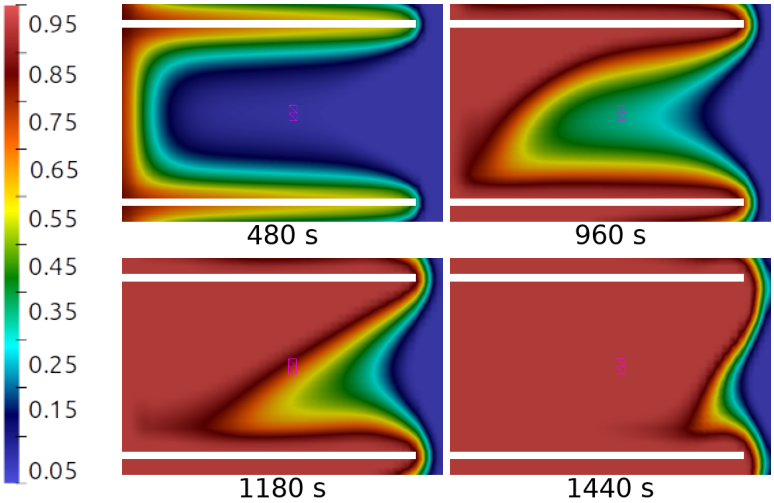

(b)

Figure 6: Temperature profiles (a) and liquid fraction distributions (b) between the 2 fins at section B on the heat exchanger during the heat charging process.

It is worth mentioning that natural convection deforms the melting front, resulting in asymmetry of the front with respect to radial axis between fins. This asymmetry is slightly seen at instant

960 s, where natural convection is not yet developed. However, from instant 1180 s, as shown in Fig. 5a, natural convection is important. The domain between the fins is separated in two by a diagonal, the entire left part of this line is melted, while the right part is still melting. This is due to the buoyancy forces modelled through the Boussinesq approximation. When a sufficient amount of liquid is present between the fins to obtain a thermal gradient, the liquid PCM heats up as it moves upwards along the tubes and cools downs as it descends along the melting front. As the liquid fraction increases, the velocity gradients (Fig. 5a) increases and the movement progressively deform the melting front as the charging process occurs.

At instant 1440 s, the slope of the numerical temperature curve in B_1 slows down before accelerating again when the PCM on the periphery of the fins completes its phase change. As long as it is not melted, the inertia of the PCM at the fin periphery slows down the overheating of the PCM between the fins.

4.6. Solidification front evolution

Fig. 7b shows the liquid fraction distribution between two fins at the section B, the squares represent the sensors location B_1 and B_2 which temperatures are shown in Fig. 7a.

Until instant 290 s, the temperature in B_1 and B_2 is the same until an inflection point is reached at 47 °C. The entire domain is liquid at almost an homogeneous temperature proximate to the liquidus point. From that point on, the PCM in the inter fin area solidifies at around the same time, where at instant 700 s no more liquid PCM is seen where all the domain possesses a liquid fraction inferior than 1. However, the PCM that is contiguous to the cold source (tubes and fins) solidified at a faster rate, generating a solidification front. The solidification front continues to advance between 700 s and 1000 s. As opposed to the melting process, the front preserves a regular shape due to the lack of natural convection. From instant 1000 s to 1440 s, the temperature

decrease rate in B_1 starts to accelerate slightly. This is because the front that leaves the wall of the tube is perpendicular to it, while the front that develops around the fins forms an arc. The profile of the thickness of the solid layer changes over time. From convex (1000 s) to the fin, it becomes concave where the inflection point is observed numerically in B_1 at instant 1440 s. The numerical and experimental temperature values are respectively 39 °C and 35 °C. As the temperatures drop below this point, the temperature decrease trend accelerates again, because the PCM is now solid and only sensitive cooling is involved, which is slower experimentally than numerically. This can be explained by the thermal contact resistance between the exchanger and solid PCM. In fact, since the PCM shrinks in volume, the solidification leads to void spaces between the fin and the PCM. Finally, at instant 1600 s, the slope of the curves slows down before accelerating again. This is caused when the PCM, at the periphery of the fins, is completely solidified, where the temperature in B_2 is 39 °C. The same conclusion is drawn by Bayón et al.[43] analysing the experimental behavior of a finned latent heat storage prototype. They find that if the volume of PCM that is far from the fins is not melted, it slows down the melting of the PCM adjacent to the fins.

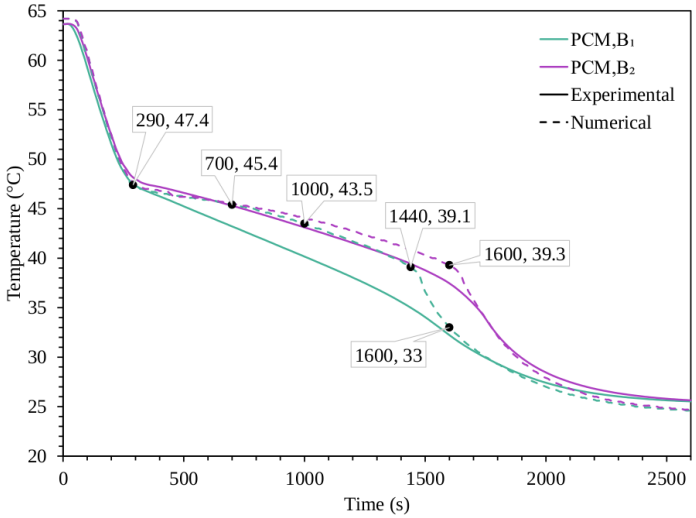

(a)

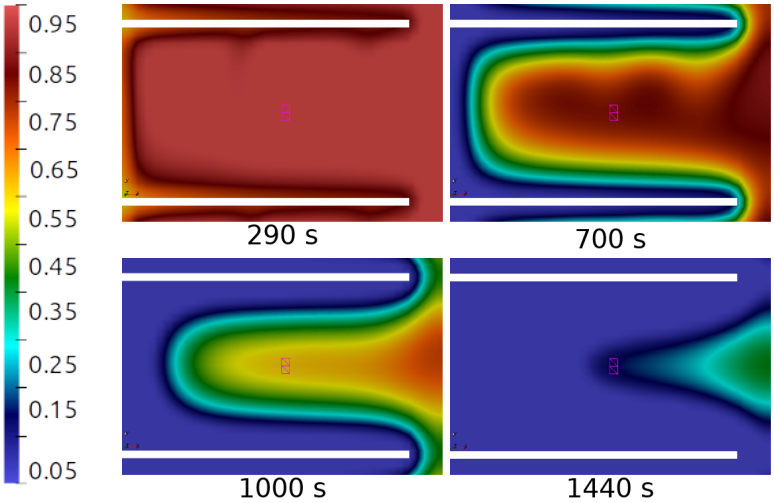

(b)

Figure 7: Temperature profiles (a) and liquid fraction distributions (b) between the 2 fins at section B on the heat exchanger during the heat discharging process.

Despite the fact that the different heat transfer properties were seen between liquid and solid phases for the paraffin studied, these were left aside in the discussion to emphasize the importance

of buoyancy movements. The influence of natural convection has always been a topic of discussion in latent heat storage systems. Some authors neglected the effect of local natural convection upon phase change process [44, 32], others argue that the contribution of natural convection is not negligible [45, 17]. For the particular geometry and paraffin studied, natural convection was key to explain the shape of the temperature profile.

5. Conclusions

The thermal behaviour of paraffins which melt in a wide temperature range inside a finned shell-and-tube heat exchanger was experimentally and numerically investigated. The effect of natural convection and phase transition temperature range of a paraffin on the melting and solidification fronts inside a finned tube heat exchanger are investigated. The main conclusions are drawn as follows:

- Due to the fact that heat transfer during charging in the shell-and-tube exchanger is largely affected by natural convection, experimental results exhibit discrepancies between the melting temperatures profiles obtained through *T-history* and experiments on the storage unit. However, they are similar for the solidification temperature profiles because the discharging process is dominated by conduction.

- As the melting process occurs, the solid paraffin is exposed to the liquid PCM at a higher temperature due to the different liquidus and solidus temperatures generating the rapid rise of temperature observed experimentally.

- Numerical results of the melting between two fins show that an arch-like melting front propagates outwardly from the tube towards the shell is observed for the paraffin between the

fins. As the liquid fraction increases, natural convection is triggered on. The melt phase with high temperature flows upwardly and enhances heat transfer between the melt and the solid paraffin, progressively deform the melting front.

References

References

[1] A. Sharma, V. V. Tyagi, C. R. Chen, D. Buddhi, Review on thermal energy storage with phase change materials and applications, Renewable and Sustainable Energy Reviews 13 (2) (2009) 318–345. arXiv:1008.0209v1, doi:10.1016/j.rser.2007.10.005.

[2] L. Karim, F. Barbeon, P. Gegout, A. Bontemps, L. Royon, New phase-change material components for thermal management of the light weight envelope of buildings, Energy and Buildings 68 (2014) 703–706. doi:10.1016/j.enbuild.2013.08.056.
URL https://linkinghub.elsevier.com/retrieve/pii/S0378778813005537

[3] L. Long, H. Ye, Y. Gao, R. Zou, Performance demonstration and evaluation of the synergetic application of vanadium dioxide glazing and phase change material in passive buildings, Applied Energy 136 (2014) 89–97. doi:10.1016/J.APENERGY.2014.09.007.
URL https://www.sciencedirect.com/science/article/pii/S0306261914009544

[4] W.-m. Guan, J.-h. Li, T.-t. Qian, X. Wang, Y. Deng, Preparation of paraffin/expanded vermiculite with enhanced thermal conductivity by implanting network carbon in vermiculite layers, Chemical Engineering Journal 277 (2015) 56–63. doi:10.1016/J.CEJ.2015.04.077.
URL https://www.sciencedirect.com/science/article/pii/S1385894715005677

[5] M. Martinelli, F. Bentivoglio, R. Couturier, J.-F. Fourmigué, P. Marty, Experimental study of an externally finned tube with internal heat transfer enhancement for phase change thermal energy storage, Journal of Physics: Conference Series 745 (3) (2016) 032029. doi:10.1088/1742-6596/745/3/032029.

[6] K. Merlin, Caractérisation thermique d'un matériau à changement de phase dans une structure conductrice, Phd thesis, Université Bretagne Loire (2016).

[7] J. Gasia, L. Miró, A. de Gracia, C. Barreneche, L. F. Cabeza, Experimental evaluation of a paraffin as phase change material for thermal energy storage in laboratory equipment and in a shell-and-tube heat exchanger, Applied Sciences 6 (5) (2016) 112. doi:10.3390/app6040112.

[8] K. Pielichowska, K. Pielichowski, Phase change materials for thermal energy storage, Progress in Materials Science 65 (2014) 67–123. doi:10.1016/j.pmatsci.2014.03.005.

[9] L. F. Cabeza, A. Castell, C. Barreneche, A. De Gracia, A. I. Fernández, Materials used as PCM in thermal energy storage in buildings: A review, Renewable and Sustainable Energy Reviews 15 (3) (2011) 1675–1695. doi:10.1016/j.rser.2010.11.018.

[10] M. Akgün, O. Aydin, K. Kaygusuz, Experimental study on melting/solidification characteristics of a paraffin as PCM, Energy Conversion and Management 48 (2) (2007) 669–678. doi:10.1016/j.enconman.2006.05.014.

[11] M. M. Farid, A. Kanzawa, Thermal Performance of a Heat Storage Module Using PCM's With Different Melting Temperatures: Mathematical Modeling, Journal of Solar Energy Engineering 111 (2) (1989) 152. doi:10.1115/1.3268301.

[12] P. Lamberg, R. Lehtiniemi, A. M. Henell, Numerical and experimental investigation of melting

and freezing processes in phase change material storage, International Journal of Thermal Sciences 43 (3) (2004) 277–287. doi:10.1016/j.ijthermalsci.2003.07.001.

[13] M. Medrano, M. O. Yilmaz, M. Nogués, I. Martorell, J. Roca, L. F. Cabeza, Experimental evaluation of commercial heat exchangers for use as PCM thermal storage systems, Applied Energy 86 (10) (2009) 2047–2055. doi:10.1016/j.apenergy.2009.01.014.

[14] I. Jmal, M. Baccar, Numerical study of PCM solidification in a finned tube thermal storage including natural convection, Applied Thermal Engineering 84 (2015) 320–330. doi:10.1016/j.applthermaleng.2015.03.065.

[15] W. W. Wang, L. B. Wang, Y. L. He, Parameter effect of a phase change thermal energy storage unit with one shell and one finned tube on its energy efficiency ratio and heat storage rate, Applied Thermal Engineering 93 (2016) 50–60. doi:10.1016/j.applthermaleng.2015.08.108.

[16] M. Esapour, M. J. Hosseini, A. A. Ranjbar, Y. Pahamli, R. Bahrampoury, Phase change in multi-tube heat exchangers, Renewable Energy 85 (2016) 1017–1025. doi:10.1016/j.renene.2015.07.063.

[17] X. Yang, Z. Lu, Q. Bai, Q. Zhang, L. Jin, J. Yan, Thermal performance of a shell-and-tube latent heat thermal energy storage unit: Role of annular fins, Applied Energy 202 (2017) 558–570. doi:10.1016/j.apenergy.2017.05.007.

[18] K. Kant, A. Shukla, A. Sharma, P. H. Biwole, Melting and solidification behaviour of phase change materials with cyclic heating and cooling, Journal of Energy Storage 15 (2018) 274–282. doi:10.1016/j.est.2017.12.005.

[19] P. Sivasamy, A. Devaraju, S. Harikrishnan, Review on Heat Transfer Enhancement of Phase Change Materials (PCMs), Materials Today: Proceedings 5 (6) (2018) 14423–14431. doi:10.1016/j.matpr.2018.03.028.

[20] S. Madruga, J. Curbelo, Dynamic of plumes and scaling during the melting of a Phase Change Material heated from below, International Journal of Heat and Mass Transfer 126 (2018) 206–220. doi:10.1016/j.ijheatmasstransfer.2018.05.075.

[21] K. Biswas, Y. Shukla, A. Desjarlais, R. Rawal, Thermal characterization of full-scale PCM products and numerical simulations, including hysteresis, to evaluate energy impacts in an envelope application, Applied Thermal Engineering 138 (January) (2018) 501–512. doi:10.1016/j.applthermaleng.2018.04.090.

[22] M. Longeon, A. Soupart, J. F. Fourmigué, A. Bruch, P. Marty, Experimental and numerical study of annular PCM storage in the presence of natural convection, Applied Energy 112 (2013) 175–184. doi:10.1016/j.apenergy.2013.06.007.

[23] A. Soupart-caron, Stockage de chaleur dans les Matériaux à Changement de Phase, Phd thesis, Université Grenobles Alpes (2015).

[24] F. Colella, A. Sciacovelli, V. Verda, Numerical analysis of a medium scale latent energy storage unit for district heating systems, Energy 45 (1) (2012) 397–406. doi:10.1016/j.energy.2012.03.043.

[25] Z. Yinping, J. Yi, A simple method, the T-history method, of determining the heat of fusion, specific heat and thermal conductivity of phase-change materials, Measurement Science and Technology 10 (3) (1999) 201–205. doi:10.1088/0957-0233/10/3/015.

[26] A. Lázaro, E. Günther, H. Mehling, S. Hiebler, J. M. Marín, B. Zalba, Verification of a T-history installation to measure enthalpy versus temperature curves of phase change materials, Measurement Science and Technology 17 (8) (2006) 2168–2174. doi:10.1088/0957-0233/17/8/016.

[27] C. Rathgeber, H. Schmit, P. Hennemann, S. Hiebler, Calibration of a T-History calorimeter to measure enthalpy curves of phase change materials, Measurement Science and Technology 25 (3) (2014) 35011. doi:10.1088/0957-0233/25/3/035011.

[28] J. M. Marín, B. Zalba, L. F. Cabeza, H. Mehling, Determination of enthalpy-temperature curves of phase change materials with the temperature-history method: Improvement to temperature dependent properties, Measurement Science and Technology 14 (2) (2003) 184–189. doi:10.1088/0957-0233/14/2/305.

[29] Z. N. Meng, P. Zhang, Experimental and numerical investigation of a tube-in-tank latent thermal energy storage unit using composite PCM, Applied Energy 190 (2017) 524–539. doi:10.1016/j.apenergy.2016.12.163.

[30] B. Metais, E. R. G. Eckert, Forced, Mixed, and Free Convection Regimes, Journal of Heat Transfer 86 (2) (1964) 295. doi:10.1115/1.3687128.

[31] The OpenFOAM Foundation, OpenFOAM v6.
URL https://openfoam.org/

[32] M. Martinelli, Stockage d'énergie thermique par changement de phase – Application aux réseaux de chaleur, Phd thesis, Université Grenobles Alpes (2006).

[33] H. Niyas, S. Prasad, P. Muthukumar, Performance investigation of a lab–scale latent heat

storage prototype – Numerical results, Energy Conversion and Management 135 (2017) 188–199. doi:10.1016/j.enconman.2016.12.075.

[34] V. R. Voller, C. Prakash, A fixed grid numerical modelling methodology for convection-diffusion mushy region phase-change problems, International Journal of Heat and Mass Transfer 30 (8) (1987) 1709–1719. arXiv:NIHMS150003, doi:10.1016/0017-9310(87)90317-6.

[35] E. Bender, Numerical heat transfer and fluid flow. VonS. V. Patankar. Hemisphere Publishing Corporation, Washington - New York - London. McGraw Hill Book Company, New York 1980. 1. Aufl., 197 S., 76 Abb., geb., DM 71,90, Vol. 53, Hemisphere Publishing Corp., Washington, 1981. doi:10.1002/cite.330530323.

[36] J. Boussinesq, Th{é}orie de l'{é}coulement tourbillonnant et tumultueux des liquides dans les lits rectilignes a grande section, Gauthier-Villars et Fils, Paris, 1897.

[37] A. D. Brent, V. R. Voller, K. J. Reid, Enthalpy-porosity technique for modeling convection-diffusion phase change: Application to the melting of a pure metal, Numerical Heat Transfer 13 (3) (1988) 297–318. doi:10.1080/10407788808913615.

[38] C. R. Swaminathan, V. R. Voller, On the enthalpy method, International Journal of Numerical Methods for Heat & Fluid Flow 3 (3) (1993) 233–244. doi:10.1108/eb017528.

[39] R. R. Kasibhatla, A. König-Haagen, F. Rösler, D. Brüggemann, Numerical modelling of melting and settling of an encapsulated PCM using variable viscosity, Heat and Mass Transfer/Waerme- und Stoffuebertragung 53 (5) (2017) 1735–1744. doi:10.1007/s00231-016-1932-0.

[40] R. Issa, A. Gosman, A. Watkins, The computation of compressible and incompressible recirculating flows by a non-iterative implicit scheme, Journal of Computational Physics 62 (1) (1986)

66–82. doi:10.1016/0021-9991(86)90100-2.

URL https://www.sciencedirect.com/science/article/pii/0021999186901002

[41] B. Launder, B. Sharma, Application of the energy-dissipation model of turbulence to the calculation of flow near a spinning disc, Letters in Heat and Mass Transfer 1 (2) (1974) 131–137. doi:10.1016/0094-4548(74)90150-7.

URL https://www.sciencedirect.com/science/article/pii/0094454874901507

[42] Rubitherm Technologies GmbH, PCM RT-LINE (2017).

URL https://www.rubitherm.eu/en/index.php/productcategory/organische-pcm-rt

[43] R. Bayón, E. Rojas, L. Valenzuela, E. Zarza, J. León, Analysis of the experimental behaviour of a 100 kWth latent heat storage system for direct steam generation in solar thermal power plants, Applied Thermal Engineering 30 (17-18) (2010) 2643–2651. doi:10.1016/J.APPLTHERMALENG.2010.07.011.

URL https://www.sciencedirect.com/science/article/pii/S1359431110002942

[44] A. Sciacovelli, F. Gagliardi, V. Verda, Maximization of performance of a PCM latent heat storage system with innovative fins, Applied Energy 137 (2015) 707–715. doi:10.1016/j.apenergy.2014.07.015.

[45] Y. Tao, Y. He, Effects of natural convection on latent heat storage performance of salt in a horizontal concentric tube, Applied Energy 143 (2015) 38–46. doi:10.1016/J.APENERGY.2015.01.008.

URL https://www.sciencedirect.com/science/article/pii/S0306261915000148

Cover Letter

Dr. Jinyue Yan
Editor-in-Chief
Journal of Applied Energy

November 26, 2018

Dear Dr. Jinyue Yan:

I am pleased to submit an original research article entitled "*Experimental and numerical study of a paraffin with a wide-range phase change for thermal energy storage*" by Cecil Vega, Oscar Pinto and Alfredo Gordon, for publication in Journal of *Applied Energy*.

One of the most commonly studied phase change materials (PCMs) are paraffins. However, due to the high cost of manufacturing, only technical grade paraffins, which are essentially paraffin mixtures and are not completely refined oils, are used as PCMs for latent heat storage storage (LTES) purposes. Moreover, previous studies evaluating the viability of technical paraffins are scarce and exhibit differences between the melting period in the temperature profiles recorded in the storage unit and in characterization.

Therefore, the present study aims to deal with this observations by taking in a depth look at the temperature profiles observed by a technical grade paraffin. To this end, the paraffin was characterized and tested in a finned shell-and-tube heat exchanger. The experimental test section is numerically modeled on the open source framework OpenFOAM and the melting and solidification fronts between fin-formed space are analysed.

The results demonstrated that local natural convection is key to explain the shape of the temperature profiles. It deforms the melting front, resulting in asymmetry of the front with respect to radial axis between fins. Moreover, as the melting process occurs, the solid paraffin is exposed to the liquid PCM at a higher temperature due to the different liquidus and solidus temperatures generating the rapid rise of temperature observed experimentally.

We believe that this manuscript is appropriate for publication by Journal of *Applied Energy* because it deals with the phenomenological effects of technical grade paraffins for LTES purposes as a medium to improve the conservation and management of energy, which is a special concern for this journal.

This manuscript has not been published and is not under consideration for publication elsewhere. All authors approved the manuscript and this submission. We have no conflicts of interest to disclose.

Thank you for receiving our manuscript and considering it for review. We appreciate your time and look forward to your response.

Thank you for your consideration!

Sincerely,

Cecil Vega
Chemical Engineer
Unidad de Desarrollo Tecnologico - UDT / Universidad de Concepcion
Concepcion, CHILE
E-mail address: ceanver@pm.me/cevega@udec.cl